STUDIES ON THE OPTIMUM FLAP DEFLECTION ANGLE OF VORTEX FLAPS

Kenichi RINOIE
Department of Aeronautics and Astronautics, University of Tokyo
Bunkyo-ku, Tokyo, 113, Japan

Toshimi FUJITA, Akihito IWASAKI and Hirotoshi FUJIEDA
National Aerospace Laboratory
6-13-1 Osawa, Mitaka, Tokyo, 181, Japan

Abstract

Low speed wind tunnel measurements were made on a 70° delta wing with leading-edge vortex flaps. Improvements in the lift/drag ratio were observed in a 70° delta wing by deflecting the leading-edge vortex flap. Comparisons between the previously measured 60° delta wing results and the present results were made. The improvements in the lift/drag ratio of the 70° delta wing were attained at a narrower lift coefficient region than that of the 60° delta wing. The present results suggest that the maximum lift/drag ratio for the 70° delta wing was attained when a spanwise length of a separated region formed on the vortex flap surface coincided with the flap width. Discussion on the optimum flap deflection angle which attained the maximum lift/drag ratio for different sweepback angle wings was also made.

Nomenclature

b	Local span, m
Cr	Wing center-line chord, m
C_D	Drag coefficient
C_L	Lift coefficient
Cp	Pressure coefficient
L/D	Lift/Drag ratio
Re_{Cr}	Reynolds number based on the wing center-line chord
U_∞	Free stream velocity, m/s
x	Chordwise coordinate measured from the apex of the delta wing, m
y	Spanwise coordinate orthogonal to x, measured from the wing center-line, m
y_R	y coordinate of the deduced reattachment point of the leading-edge separation vortex, m
α	Wing angle of attack, degree
δ_f	Vortex flap deflection angle measured normal to the hinge line, degree
δ_{fs}	Streamwise vortex flap deflection angle, degree
ε	Semi apex angle of the main wing inboard the flap hinge line, degree
Λ	Model sweepback angle, degree

Introduction

The low speed aerodynamic characteristics of delta wing are known to be relatively inefficient, because the pair of leading-edge separation vortices formed on the delta wing generate a large amount of drag force (Fig.1a). The leading-edge vortex flap (LEVF) is one of the devices which can improve the aerodynamic efficiency of delta wings at low speeds[1]. The LEVF is a full span deflectable flap attached to the leading-edge of the delta wing. With the flap deflected downward, a leading-edge separation vortex is formed over the forward facing flap surface (Fig.1b). The suction force generated by the vortex acts on the flap surface and generates a thrust component. Hence it reduces the drag and improves the lift/drag ratio, an essential factor for the improvement of the take-off and climb performance of the delta wing aircraft, one of the next generation high speed civil transport aircrafts. Many tests have been made which confirm the benefit of the LEVF[2].

The first author has made experimental studies using two kinds of 60° delta wing models with tapered LEVFs which have different cross sections[3, 4]. One of the conclusions in Refs. 3 and 4 was that the highest lift/drag ratio is achieved using a modest LEVF deflection angle which causes the flow to attach on the flap surface without any large separation. This conclusion was obtained by the delta wing which has a sweepback angle Λ of 60°. It is of interest as to whether this conclusion is only applicable to a delta wing when Λ=60°. It is also important to know how the difference of the sweepback angle affects the flow around the LEVF and the aerodynamics of the wing. Therefore, further wind tunnel experiments have been made using a Λ=70° delta wing model with a tapered LEVF in a 2m x 2m low speed wind tunnel. The force, surface pressure measurements and oil flow visualization were made. The obtained results are compared with the 60° delta wing results[4]. The flow around the LEVF at the highest lift/drag ratio for 60° and 70° delta wings is discussed.

The first author conducted analytical studies[5] to estimate the aerodynamic characteristics of the delta wing with the LEVF using a quasi-vortex lattice method coupled with a leading-edge suction analogy.

Comparisons are made with experimental and analytical results of the 70° delta wing with the LEVF to confirm the experimental results.

These studies have been done mainly to understand the behavior and the benefits of the LEVF. However, the LEVF should be deflected at the flap angle so that the delta wing with the LEVF attains the best lift/drag ratio at a specific wing angle of attack, such as at a take-off and climb angle of attack. This means that a method to predict the optimum flap deflection angle, which attains the maximum lift/drag ratio at any fixed angle of attack, is needed for practical purposes. Discussion of the optimum flap deflection angle is also made in this paper.

70° Delta Wing with Vortex Flaps

Experimental Details

Fig.2 shows the model details. The model is a 70° flat plate delta wing with no camber. The center-line chord length Cr is 0.5m and the thickness is 0.015m. The upper and lower surfaces of all the edges are cut away so that the edges are sharp and have an apex angle of 8.6° at two leading-edges and 12.8° at a trailing-edge, where the angle is measured in a plane normal to the edge concerned. The model has the LEVF hinge lines running from the wing apex to 75% of the trailing-edge semispan station. Three rows of pressure tapping were located on the upper surface and one row on the lower surface. The flap deflection angle δ_f is defined as the angle measured in the plane normal to the hinge line. Different flap deflections of δ_f=0° to 50°, with an increment of 10°, were tested.

The experiments were made in a 2m x 2m low speed, closed working section, closed return wind tunnel at the National Aerospace Laboratory in Japan. All tests were done at a tunnel speed of U_∞ = 30m/s. The Reynolds number based on the wing center line chord Re_{Cr} was 1×10^6. The angle of attack α was increased from -10° to 42°. The model was mounted on a shielded strut with a tail sting. To account for interference between the strut and the model, which was observed in Refs 3 and 4, the interference correction using a dummy strut[6] was made in the angle of attack range from -10° to 10°. Tunnel boundary corrections were applied to the measured data using the same procedure described in Ref.3. Surface pressure measurements were made using Electronically Scanner Pressure Sensors (ESP). A flow visualization test using the surface oil flow was conducted to describe the flow around the LEVF.

Experimental Results

The C_L vs. α curves are shown in Fig.3 for various δ_f. Results with strut interference correction are shown in $-10° < \alpha \leq 10°$ and results without strut interference correction in $\alpha > 10°$. Therefore, there are gaps at α=10° in Fig.3. This figure shows that the C_L for δ_f=0°, i.e. a symmetrical flat delta wing, is zero at α=0°. This means that the strut interference has been corrected properly. This figure shows that the C_L decreases as the LEVF is deflected downwards. This trend is the same as that reported in Refs.3 and 4. The C_D-α curves (Fig.4) show the C_D decreases for most of the positive α region, as δ_f increases.

Fig.5 shows the lift to drag ratio (L/D) versus C_L. The results with strut interference correction are shown in the C_L range of $C_L \leq 0.4$ and results without correction in the C_L range of $C_L > 0.4$. A large L/D improvement for δ_f=20° and 30° are seen at about C_L=0.2~0.3. The observed maximum L/D is 11.8, which is attained at δ_f=20°, α=5°. The L/D for all δ_f in the C_L range greater than 0.5 show almost the same L/D distributions, which means that there is no benefit in using a LEVF for C_L's > 0.5.

Fig.6 shows surface pressure distributions for the upper surface at x/Cr=0.55. Figs.6a and 6b show that the leading-edge separation vortex is formed at α=9° for δ_f=0° (Fig.6a) and for δ_f=30° (Fig.6b). The spanwise length of the leading-edge separation vortex for δ_f=30° (Fig.6b) is shorter than that for δ_f=0° (Fig.6a) at this angle of attack. Fig.6c shows the Cp distributions for the wing with δ_f=50°. The spanwise length of the vortex at α=9° is much shorter than that for the δ_f=30° at α=9°. The suction region is seen inboard the flap hinge line ($y/(b/2)$=0.5 ~0.75) at α=6°, 9° and 12° in Fig.6c. This means that a separation region is formed inboard the hinge line.

Fig.7 shows the surface flow patterns sketched from oil flow pictures of the upper surface of the left wing at α=9°. In these figures, H.L. denotes the hinge line. The patterns define the vortex positions on the wing and flap surfaces. In Figs.7a and 7b, the leading-edge separation vortex is clearly recognized. A vortex is formed inboard the flap hinge line for the wing with δ_f=50° (Fig.7c). These results agree with surface pressure measurements in Fig.6.

Comparisons between the 60° and 70° Delta Wings

The 60° delta wing model used in Ref.4 and the present 70° delta wing model have similar planar shapes except for the sweepback angle, but they have different cross-sections. Measurements were made at different Reynolds numbers. The 60° delta wing model used in Ref.4 has a symmetrical smooth convex cross-section. Measurements in Ref.4 were made at Re_{Cr} = 2×10^6. However, it is known that both the aerodynamic characteristics of the sharp leading-edge delta wing and the behavior of the leading-edge separation vortex formed on the delta wing are not so affected by differences in the model cross-section and in the Reynolds number. See e.g., Ref.7. Therefore, it was concluded that the effect of

the sweepback angle upon the LEVF characteristics could be investigated by comparing the present results with Ref.4's results. In this section, the geometrical angle of attack as measured from the tunnel center-line without any tunnel wall correction is used to define the angle of attack of the model.

Lift/Drag Ratio

Figs.8a and 8b show the L/D - C_L distributions for the wing with δ_f=0° and δ_f=30° of the 60° delta wing (Fig.8a) and of the 70° delta wing (Fig.8b). Fig.8a shows that the L/D of the 60° delta wing with δ_f=30° is greater than that of the δ_f=0° wing in the C_L range between 0.15 and 0.6. Fig.8b shows the L/D benefit of the 70° delta wing with δ_f=30° is seen in the C_L range only between 0.1 and 0.25. The C_L range in which the L/D is improved for the 70° delta wing is narrower than that for the 60° delta wing.

Spanwise Length of Leading-Edge Separation Vortex

Figs.9a and 9b show the spanwise length of the leading-edge separation vortex vs. α curves at different δ_f for 60° and 70° delta wings. The reattachment point of the leading-edge separation vortex was deduced from the surface pressure measurements, as shown in Fig.9a. The spanwise coordinate y_R measured from the wing center line is plotted in Fig.9 as a reattachment point of the vortex. The Cp results at x/Cr=0.4 for the 60° delta wing and Cp's at x/Cr=0.55 for the 70° wing were used to draw Fig.9. The distance between the reattachment point and the wing tip ($y_R/(b/2)$=1.0) denotes the spanwise length of the leading-edge separation vortex. The fact that the reattachment point coincides with the wing tip position at the same angles of attack in Fig.9 means that the leading-edge separation vortex has not yet been formed on the wing surface at these angles of attack. Comparisons between Figs.9a and 9b show that the leading-edge separation vortex on the 70° delta wing begins to form at smaller angle of attack than that of the 60° delta wing, when the wing angle of attack is increased from α=0°. The streamwise angle formed between the free stream and the flap surface of the 70° delta wing is larger than that of the 60° delta wing when compared at the same α and δ_f, because of the difference in the model sweepback angle. This means that the separation occurs at smaller angle of attack for the 70° delta wing than that for the 60° delta wing at the same δ_f.

Flow around the LEVF at the optimum L/D

In this section, the flow pattern around the LEVF, when the wing attains its absolute maximum L/D, is discussed. Fig.10 shows the surface pressure distributions at the maximum L/D wing configuration measured at different chord stations. Since small errors in measuring C_D can have a large influence on the maximum L/D calculated, some Cp distributions of wing configurations which attain both the absolute maximum L/D and the near maximum L/D are shown in the figure.

Fig.10a shows the pressure distributions of the 60° delta wing for three wing configurations, i.e. three combinations of δ_f and α. Results at x/Cr=0.4 and 0.8 are shown. Except for when δ_f=15°, α=6°, x/Cr=0.4, Cp distributions are almost flat for all the spanwise stations. This means that no large separation occurs on either the LEVF or the wing surfaces of the 60° delta wing at the maximum L/D configuration. Therefore, it was concluded in Ref.4 that the highest value of L/D is achieved when the flow attaches on the LEVF surface without any large separation on the 60° delta wing.

Fig.10b shows the Cp of the 70° delta wing. Results at x/Cr=0.4 and 0.55 show similar distributions. A suction region is seen at $y/(b/2)$=0.75 ~1.0 for every wing configuration. This means that a separation region is formed on the wing at the maximum L/D configuration. The spanwise length of this separation region almost coincides with the flap width. It is noted the maximum $|-Cp|$ value in this figure is not so high when compared with that at higher angle of attack when the leading-edge separation vortex is formed on the delta wing without flap deflections (see Fig.6a).

Comparisons between the Experimental and Analytical Results

Aerodynamic characteristics of the 60° delta wing with the LEVF were estimated in Ref.5. Details of the analytical method used are described in Ref.5. Only a brief description of the method is presented here.

The complex behaviors of the leading-edge separation vortex formed on the LEVF were experimentally similar to the vortex on a plain delta wing[3,4]. This led to the analytical model of the separation vortex on the LEVF using the leading-edge suction analogy[8]. The leading-edge suction analogy assumes that the amount of the suction caused by the leading-edge separation vortex on the delta wing is equal to the amount of the leading-edge suction force calculated from the potential flow theory when there is no vortex. For the case of the wing with the LEVF, the amount of the leading-edge thrust force was assumed to act normally on the flap surface as a vortex suction force. A quasi-vortex lattice method[9] (QVLM) was used to estimate this leading-edge thrust force. By combining the suction analogy and the QVLM, the C_L and C_D of the delta wing with the LEVF were estimated. This method is basically similar to the methods in Refs. 10 and 11. The aerodynamic characteristics of the 70° delta wing with the LEVF were estimated by this method.

Figs.11 and 12 compare the results of the experiments with those of this analytical method for the 60° and 70° delta wing with LEVF deflection angles δ_f of 0° and 30°. In these figures, a caption "QVLM+SA"

denotes the results obtained by the present analytical method. In Fig.11, the C_L vs. α curve is shown. Fig.11a (60° delta wing, taken from Ref.5) and 11b (70° delta wing) show good agreement with the experimental results, except at a large α for the 60° delta wing (Fig.11a). In Fig.12, C_D vs. α curves are shown. In these figures, a constant value of 0.005 is subtracted from the experimentally determined C_D to compensate for the skin friction drag[5]. Again, the experimental results and analytical results are in good agreement for the 60° and 70° delta wings. Note that the strut interference for the 60° delta wing has been corrected in Figs.11 and 12, as was described in Ref.5.

Figs.11 and 12 indicate that the present analytical method accurately predicts the resultant aerodynamic characteristics of the wing with the LEVF at different sweepback angles.

Optimum Flap Deflection Angle

As stated in the introduction section, for practical purposes it is desirable to establish a method to predict the LEVF deflection angle which attains the optimum *L/D* at a given angle of attack, such as at the take-off and climb angle of attack. In this section, discussion is made on this optimum flap deflection angle, by using the experimental results of the 60° and 70° delta wings.

A streamwise flap deflection angle δ_{fs} is used as a parameter which controls the behavior of *L/D*. The δ_{fs} is derived by

$$\delta_{fs} = \tan^{-1} (\sin \varepsilon \cdot \tan \delta_f) ,$$

where ε is a semi apex angle of the main wing alone, i.e. inboard the flap hinge line. The wing configuration $\delta_{fs}=\alpha$ means that the direction of the free stream coincides with the direction of the flap surface. When $\delta_{fs} < \alpha$, the stagnation point is expected to be located on a lower surface of the flap and a separation occurs on the upper surface. When $\delta_f > \alpha$, the separation occurs on the lower surface. It is noted that the flow direction near the wing is not parallel to the direction of the free stream. Therefore, the above discussion is only a rough estimation. However, δ_{fs} may be used as a parameter representing the occurrence of separation on the flap surface.

At a fixed angle of attack, the amount of *L/D* changes as a flap deflection angle is increased from 0°. Therefore, by consulting the experimental results of the 60° and 70° delta wings, the streamwise flap deflection angle δ_{fs} at which the *L/D* attains its local maximum at the fixed angle of attack is obtained. This deflection angle is hereafter referred to as an optimum flap deflection angle. The optimum flap deflection angle was estimated at every angle of attack for the 60° and 70° delta wings. Fig.13 shows the optimum flap deflection angle δ_{fs} vs. α diagram. In this figure, the flap deflection angle, at which the difference between the *L/D* concerned and the local maximum *L/D* is less than 0.1, is also plotted as an optimum flap deflection angle to compensate for experimental errors. The hatched symbol denotes the wing configuration which attains the absolute maximum *L/D* for the delta wing concerned.

In this figure, data taken from Ref.12 is also shown. In this reference, subsonic wind tunnel experiments at Mach 0.4 have been made using a wing-body configuration with a vortex flap. The vortex flap is deflectable at about a 74° swept hinge line. Flap deflections of 0°, 30°, 40° and 45° downward were tested in the angle of attack ranges of 0° to 24°. Since the number of tested flap deflection angles is limited, the scattering of data from Ref.12 are seen in Fig.13.

Fig.13 shows that the optimum flap deflection angle distributions for different sweepback angle delta wings are similar to each other. They have a strong correlation with the $\delta_{fs}=\alpha$ line. The flow patterns around the LEVF of the different sweepback angle wings were different, as discussed in the previous section. However, this figure suggests that the optimum streamwise flap deflection angle δ_{fs} seems unaffected by the difference of the sweepback angle. More experimental data for different sweepback angles are needed to validate this hypothesis.

Conclusions

Measurements were made on a 70° delta wing with leading-edge vortex flaps. These results were compared with previously measured results on a 60° delta wing. Discussion on the optimum flap deflection angle which attains the maximum lift/drag ratio was made.

1) Improvements in the lift/drag ratio by deflecting the leading-edge vortex flap of a 70° delta wing were confirmed.

2) Comparisons between the 60° and 70° delta wings show that improvements in the lift/drag ratio of the 70° delta wing are attained at a narrower lift coefficient region than that of the 60° delta wing.

3) Previously measured results suggested that the maximum lift/drag ratio for the 60° delta wing is attained when no large separation is formed on the flap surface. However, the present results suggest that the maximum lift/drag ratio for the 70° delta wing is attained, when a separated region is formed on the vortex flap and the spanwise length of this separated region almost coincides with the vortex flap width.

4) The analytical method using the leading-edge suction analogy accurately predicts the aerodynamic characteristics of the 70° delta wing.

5) The three cases of experimental results suggest that

the optimum streamwise flap deflection angle, at which the local maximum lift/drag ratio is attained at a fixed angle of attack, is not largely affected by the difference in the wing sweepback angle.

Acknowledgement

We would like to thank Mr. Hikaru Takami, Mitsubishi Heavy Industries, Nagoya, Japan, for his beneficial advice.

References

1) Rao, D.M., "Leading-Edge Vortex-Flap Experiments on a 74 Deg. Delta wing," NASA CR-159161, Nov. 1979.

2) Campbell, J.F. and Osborn, R.F., "Leading-Edge Vortex Research: Some Nonplanar Concepts and Current Challenges," *Vortex Flow Aerodynamics Volume I*, NASA CP-2416, Jul. 1986, pp.31-63.

3)Rinoie, K., "Experiments on a 60° Delta Wing with Vortex Flaps and Vortex Plates," *The Aeronautical Journal*, Vol.97, No.961, Jan. 1993.

4) Rinoie, K. and Stollery, J.L., "Experimental Studies of Vortex Flaps and Vortex Plates," *J. Aircraft*, Vol.31, Mar.-Apr. 1994 (to be published).

5) Rinoie, K., "Estimating the Aerodynamic Characteristics of Vortex Flaps Using the Leading-Edge Suction Analogy," *Transactions of the Japan Society for Aeronautical and Space Sciences*, Vol.36, No.113, Nov. 1993, pp.143-152.

6) Rae, Jr, W.H. and Pope, A., *Low Speed Wind Tunnel Testing (2nd Edition)*, John Wiley, New York, 1984, pp.204-213.

7) Rom, J., *High Angle of Attack Aerodynamics*, Springer-Verlag, New York, 1991, pp.15-21.

8) Polhamus, E. C., "A Concept of the Vortex Lift of Sharp-Edge Delta Wings Based on a Leading-Edge Suction Analogy," NASA TN D-3767, Dec. 1966.

9) Lan, C.E., "A Quasi-Vortex-Lattice Method in Thin Wing Theory," *J. Aircraft*, Vol.11, Sep. 1974, pp.518-527.

10) Lamar, J.E., Schemensky, R.T. and Reddy, C.S., "Development of a Vortex-Lift Design Procedure and Application to a Slender Maneuver-Wing Configuration," *J. Aircraft*, Vol.18, Apr. 1981, pp.259-266.

11) Lan, C.E. and Chang, J., "Calculation of Vortex Lift Effect for Cambered Wings by the Suction Analogy," NASA CR-3449, Jul. 1981.

12) Frink, N.T., "Subsonic Wind-Tunnel Measurements of a Slender Wing-Body Configuration Employing a Vortex Flap," NASA TM-89101, Jul. 1987.

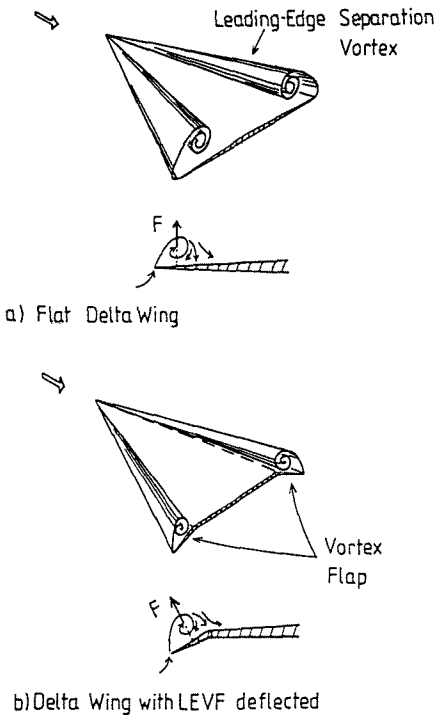

Fig.1 The Concept of a Vortex Flap[4]

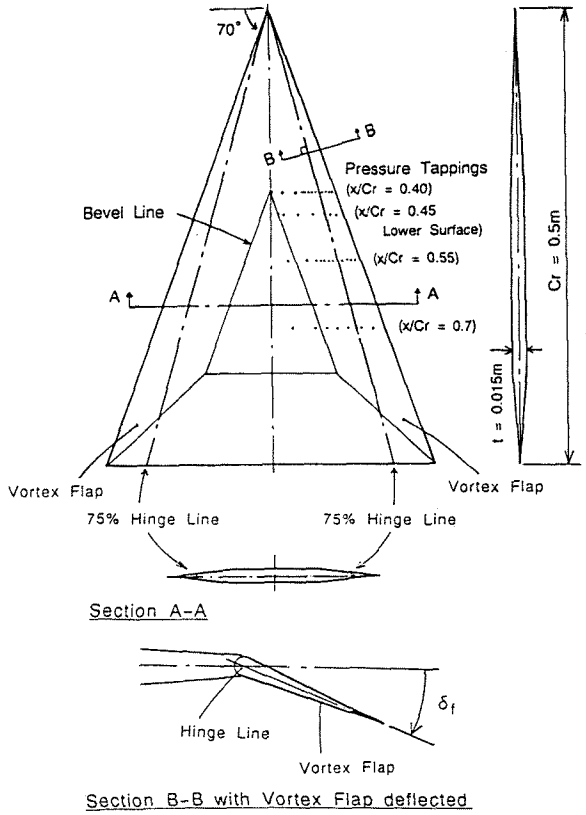

Fig.2 The Delta Wing Model with LEVF (Λ=70°)

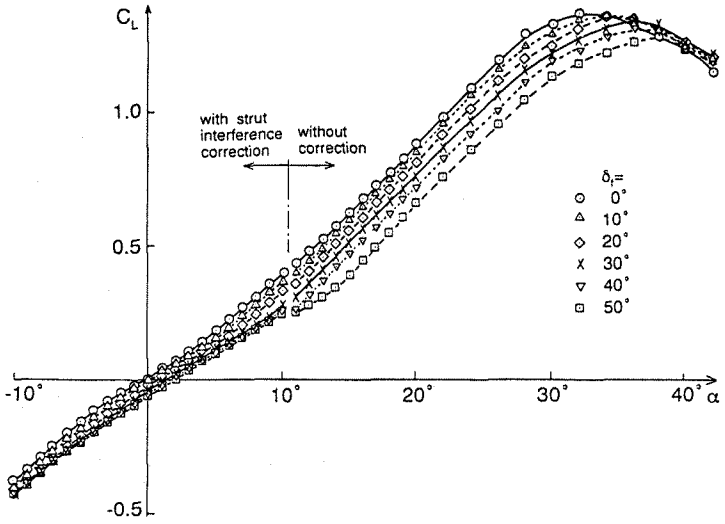

Fig.3 The Effect of the LEVF on C_L vs. α (Λ=70°)

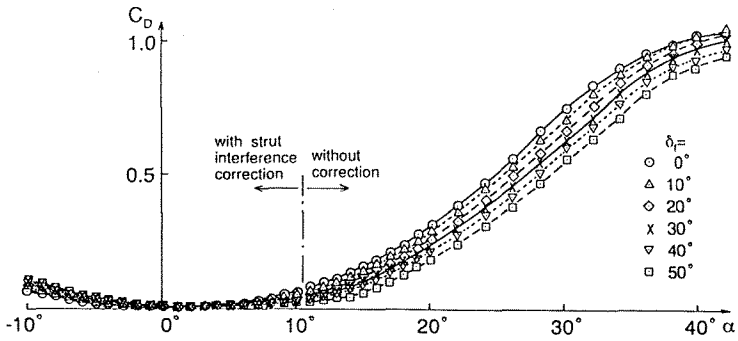

Fig.4 The Effect of the LEVF on C_D vs. α (Λ=70°)

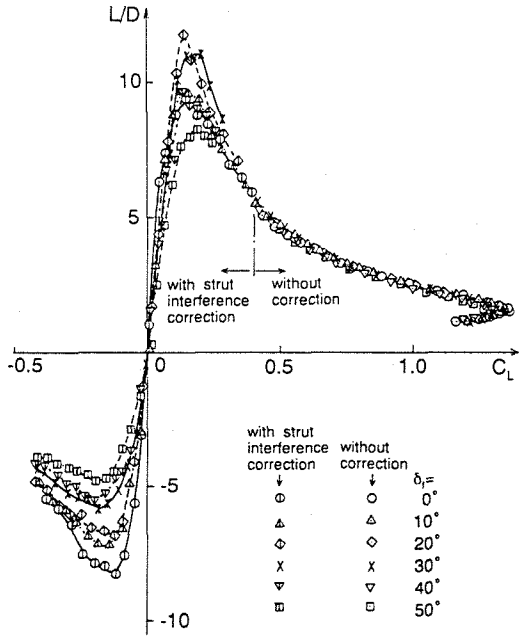

Fig.5 The Effect of the LEVF on L/D vs. C_L (Λ=70°)

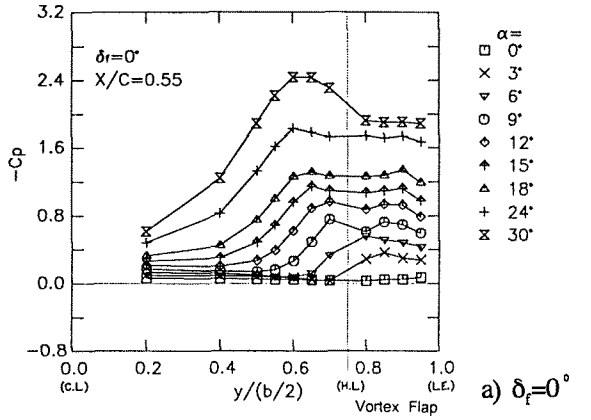

a) δ_f=0°

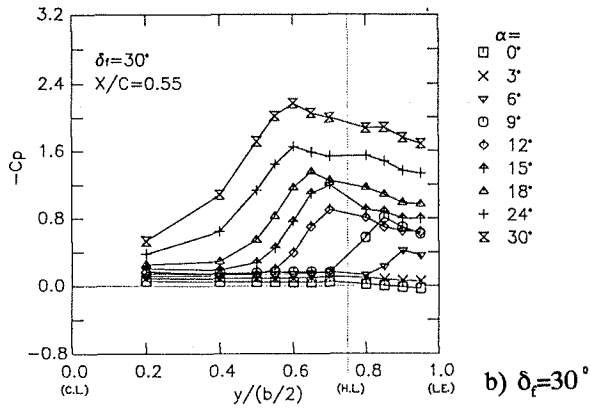

b) δ_f=30°

Fig.6 Surface Pressure Distributions at x/Cr=0.55 (Λ=70°)

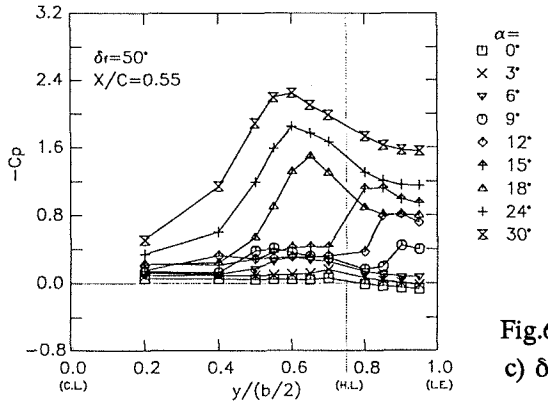

Fig.6 c) δ_f=50°

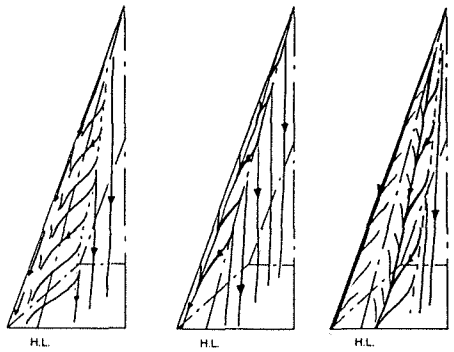

a)δ_f=0° b)δ_f=30° c)δ_f=50°

Fig.7 Surface Flow Patterns at α=9° (Λ=70°)

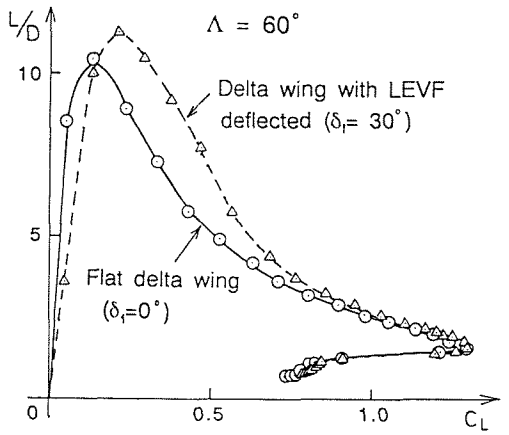

a) Λ=60°[4)]

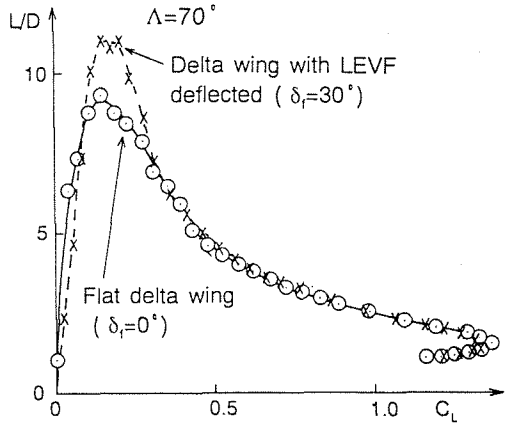

b) Λ=70°

Fig.8 L/D vs. C_L for δ_f=0° and δ_f=30°

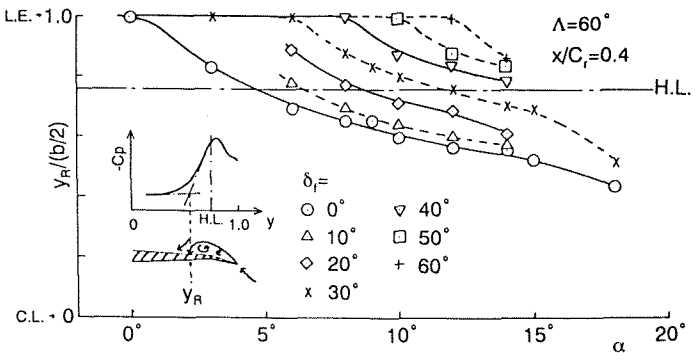

a) Λ=60°

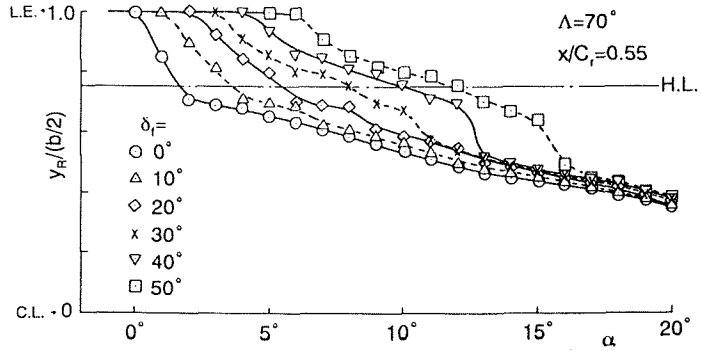

b) Λ=70°

Fig.9 The Spanwise Length of the L. E. Separation Vortex vs. α

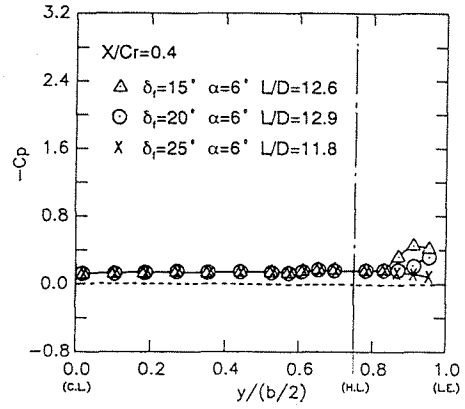

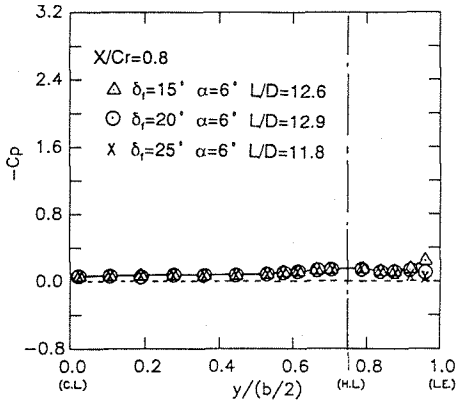

a) Λ=60°[4)]

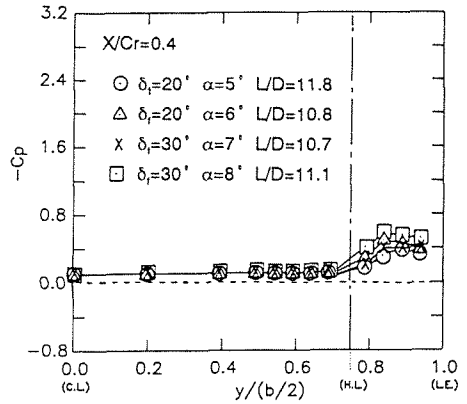

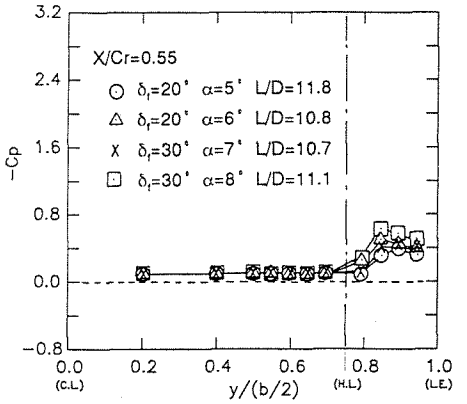

b) Λ=70°

Fig.10 Surface Pressure Distributions at the Optimum L/D Configuration

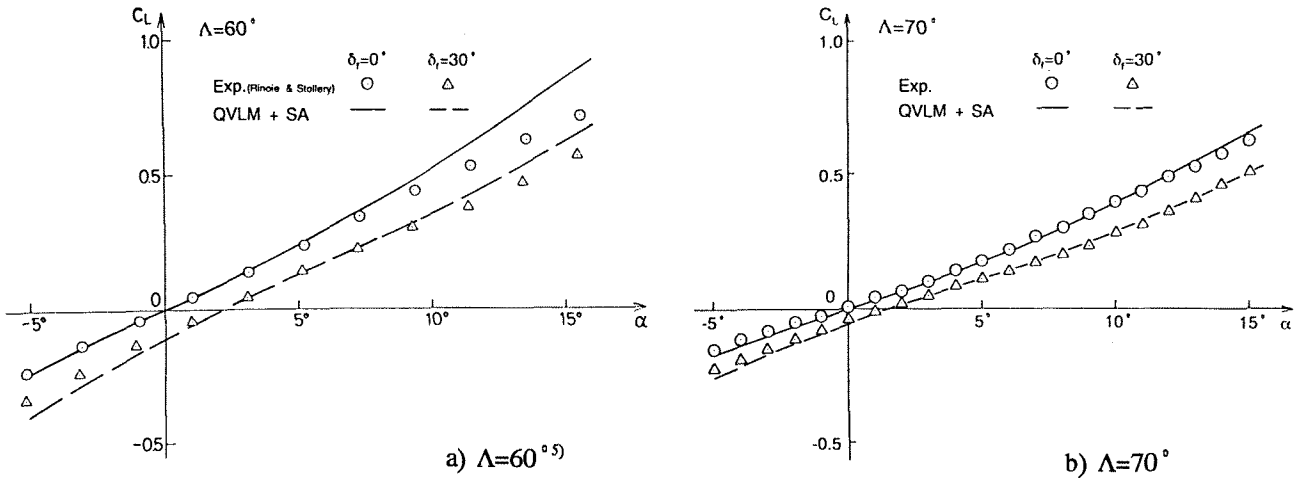

a) Λ=60°[5)]　　b) Λ=70°

Fig.11 Estimated and Experimental Curves of C_L vs. α (δ_f=0°, 30°)

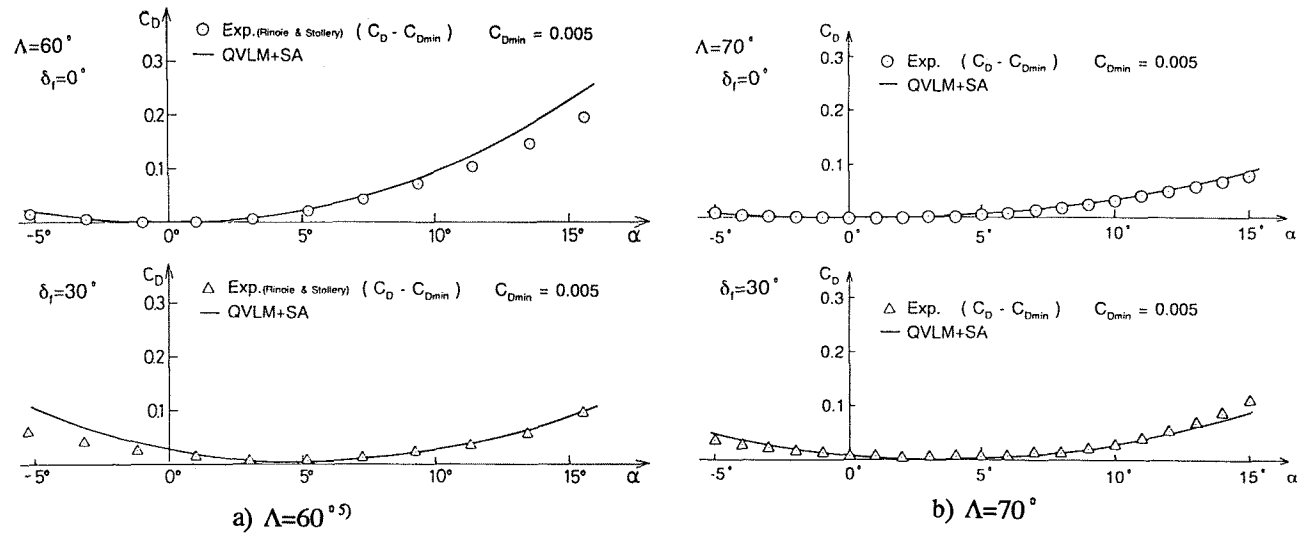

a) Λ=60°[5)]　　b) Λ=70°

Fig.12 Estimated and Experimental Curves of C_D vs. α (δ_f=0°, 30°)

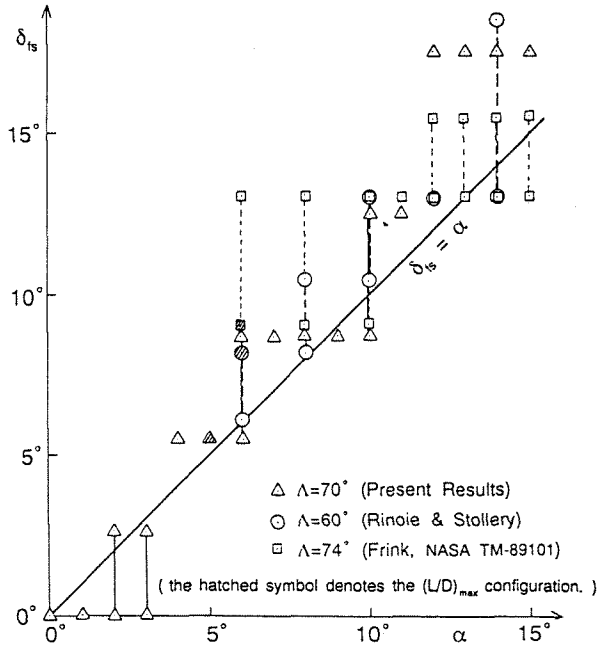

Fig.13 Optimum L/D on δ_{fs} vs. α Diagram